

Magnetic response in the underdoped cuprates

A. J. A. James,¹ R. M. Konik,^{1,*} and T. M. Rice^{1,2}

¹Condensed Matter Physics and Material Science Department, Brookhaven National Laboratory, Upton, New York 11973, USA

²Institut für Theoretische Physik, ETH Zürich, CH-8093, Zürich, Switzerland

(Received 17 January 2012; revised manuscript received 29 August 2012; published 25 September 2012)

We examine the dynamical magnetic response of underdoped cuprates by employing a phenomenological theory of a doped resonant valence bond state where the Fermi surface is truncated into four pockets. This theory predicts a resonant spin response which, with increasing energy (0 to 100 meV), appears as an hourglass. A very-low-energy spin response is found at $(\pi, \pi \pm \delta)$ and $(\pi \pm \delta, \pi)$ and is determined by scattering from the pockets' front side to the tips of opposite pockets where a van Hove singularity resides. At energies beyond 100 meV, strong scattering is seen from $(\pi, 0)$ to (π, π) . This theory thus provides a semiquantitative description of the spin response seen in both inelastic neutron scattering and resonant inelastic x-ray scattering experiments at all relevant energy scales.

DOI: [10.1103/PhysRevB.86.100508](https://doi.org/10.1103/PhysRevB.86.100508)

PACS number(s): 74.25.Ha, 74.20.Mn, 74.72.Gh

Introduction. Neutron scattering studies of the magnetic properties of underdoped cuprate superconductors have revealed an unusual “hourglass” pattern in the spin excitation spectrum that persists into the normal state.¹ This spectrum, centered on (π, π) , can be divided into three energy regions. At low energies the weight is shifted to nearby incommensurate wave vectors, peaking along the crystal axes. With increasing energy the weight moves towards (π, π) and is more uniformly distributed about this wave vector. Whether this inward dispersion reaches (π, π) depends on the particular cuprate being examined. At still higher energies a uniform ring appears evolving away from (π, π) . Recent resonant inelastic x-ray scattering (RIXS) experiments² have explored this high-energy region further.

A phenomenological theory for the underdoped pseudogap phase proposed by Yang, Rice, and Zhang (YRZ)³ has had considerable success in reproducing many electronic quasiparticle properties,⁴ both in scanning tunneling microscopy⁵ and in angle-resolved photoemission spectroscopy⁶ experiments. Heretofore, a prediction of the spin response based on this phenomenology has not been developed. In part this is because the YRZ theory was developed as a phenomenological ansatz for the single-particle Green's function (GF),³ and it was unclear how to extend it to the spin response, $S(\omega, k)$. In this article we present a derivation of the YRZ theory from a microscopic model and then use a consistent set of microscopics to calculate $S(\omega, k)$. We show that this $S(\omega, k)$ reproduces key features of the experiments just described, at all three energy scales, in particular, recent RIXS experiments.² We thus demonstrate that the YRZ phenomenology can provide a consistent description for a wide range of phenomena and energies in underdoped cuprates.

In doing so, this work entangles itself in the intensely debated question of whether the magnetic response in cuprates arises from itinerant electrons or from localized electrons.^{7,8} While we argue that the magnetic response can be explained by itinerant electrons (YRZ quasiparticles), an important body of work^{9,10} associates this magnetic phenomena with spin and charge density waves (i.e., stripes) which appear as incommensurate quasielastic peaks in the magnetic response. While we cannot decide this argument, we demonstrate that

it is possible for at least an itinerant picture to describe phenomena such as the low-energy hourglass that appears naturally in the stripe picture.

YRZ spin response. The YRZ ansatz, as originally conceived, was for the single-particle GF of underdoped cuprates. The associated Fermi surface is truncated and composed of four nodal pockets (Fig. 1) with an area proportional to the doping, x . This GF is also characterized by lines of Luttinger zeros which coincide with the magnetic Brillouin zone (BZ) or Umklapp surface¹² (see Fig. 1). The ansatz was inspired by an analysis of a system of weakly coupled Hubbard ladders where a similar phenomenology was found.¹³

To extend the YRZ ansatz to the spin response, we first elucidate the connection between YRZ and the slave boson (SB) treatment of the t - J Hamiltonian. SBs provide a natural random phase approximation (RPA)-like form for the spin response and we intend to adapt this to the assumptions of YRZ. In this way we will arrive at a form for the spin response that takes into account the same assumptions used in the YRZ form of the single-particle GF. We write the t - J Hamiltonian as

$$H = - \sum_{ij\sigma} t_{ij}^{nn} c_{i\sigma}^\dagger c_{j\sigma} - \sum_{ij\sigma} t_{ij}^{nnn} c_{i\sigma}^\dagger c_{j\sigma} + \frac{1}{2} \sum_{ij} J_H S_i \cdot S_j \quad (1)$$

$$\equiv H_t^{nn} + H_t^{nnn} + H_{J_H}.$$

The Hamiltonian is divided into terms involving nearest-neighbor NN hopping, H_t^{nn} , next-nearest-neighbor (NNN) hopping (and beyond), H_t^{nnn} , and a spin-spin interaction, H_{J_H} . We now subject $H_t^{nn} + H_{J_H}$ to the standard SB mean-field theory (SBMFT) treatment (leaving H_t^{nnn} till later). We thus factor the fermions, $c_{i\sigma}^\dagger$, into spinons $f_{i\sigma}^\dagger$ and holons b_i via $c_{i\sigma}^\dagger = f_{i\sigma}^\dagger b_i$, where the spinons and holons are subject to the constraint $\sum_\sigma f_{i\sigma}^\dagger f_{i\sigma} + b_i^\dagger b_i = 1$. At this level the spinon GF is¹⁴

$$G_\sigma^f(\omega, \mathbf{k}) = \frac{1}{\omega - \xi_0(\mathbf{k}) - \Sigma_R(\omega, \mathbf{k})}, \quad (2)$$

where $\Sigma_R = |\Delta_R(\mathbf{k})|^2 / (\omega + \xi_0(\mathbf{k}))$ and $\Delta_R(\mathbf{k}) = \Delta_0(x)(\cos k_x - \cos k_y)$. Here $t(x)$ and $\Delta_0(x)$ are doping-dependent parameters. The single-particle GF, G_σ^c , is

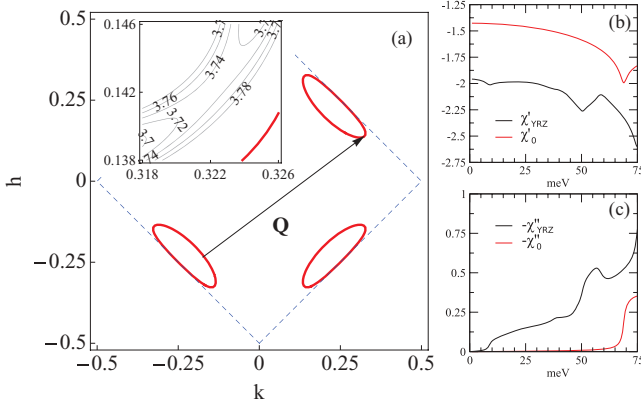


FIG. 1. (Color online) (a) The Fermi surface for hole doping, $x = 0.12$. Hole pockets are shown by solid (red) curves, while dashed (blue) lines are Luttinger zeros. Also marked is a nesting vector $\mathbf{Q} = (0.5, 0.375)$ (in reciprocal lattice units), connecting the tip of a pocket to the front side of another pocket. Inset: At the tip of the pocket there is a saddle point in the superconducting quasiparticle dispersion and hence a van Hove singularity. Energy contours are labeled in milli-electron volts. The parameters used here are $t(x) = 70$ meV, $t'(x) = -0.18t(x)$, $t''(x) = 0.12t(x)$, $\Delta_0 = 0.34t(x)$, and $\Delta_{SC} = 0.05t(x)$. (b) The real parts of $\chi_{YRZ}(\omega, \mathbf{Q})$ and $\chi_0(\omega, \mathbf{Q})$ vs ω . (c) The imaginary parts.

given directly in terms of the spinon GF because we assume that the bosons are nearly condensed, replacing the boson propagator $\langle b_i^\dagger(\tau)b_j(0) \rangle$ with $g_t(x)$: $G_\sigma^c(\omega, \mathbf{k}) = g_t(x)G_\sigma^f(\omega, \mathbf{k})$ [in the SBMFT, $g_t(x) = x$;¹⁴ in the Gutzwiller approximation, $g_t(x) = 2x/(1+x)^3$]. This differs from the YRZ form in that the full dispersion in the denominator is replaced by the dispersion due to NN hopping.

Following a recent suggestion by P. A. Lee,¹¹ we bridge the gap between the SBMFT and the YRZ, by returning to the neglected NNN hopping, H_t^{nnn} . Treating this term in the MFT moves the Luttinger zeros off the magnetic BZ and so we instead use an RPA-like approximation (Fig. 2), leading to

$$G_\sigma^f(\omega, \mathbf{k}) = \frac{1}{\omega - \xi_0(\mathbf{k}) - \xi'(\mathbf{k}) - \Sigma_R(\omega, \mathbf{k})}. \quad (3)$$

Here $\xi'(k) = -4t'(x)\cos k_x \cos k_y - 2t''(x)(\cos 2k_x + \cos 2k_y) - \mu_p$ is the dispersion due to the NNN terms and includes the fermion chemical potential. The spinon propagator in this form now gives the YRZ ansatz. The key consequence of the non-MFT treatment of the H_t^{nnn} and a central feature of our phenomenology is that spinons and holons are bound together. This binding distinguishes YRZ from the standard SBMFT approximation, which produces an expanded Hilbert space with independent spinons and holons. Lest this distinction between H_t^{nnn} and H_t^{nn} seem

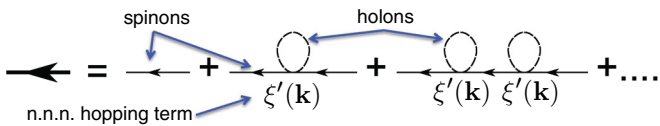


FIG. 2. (Color online) RPA form of the YRZ spinon propagator in terms of SB propagators.

artificial, we derive in Ref. 15 a YRZ-like ansatz for $G_\sigma^f(\omega, k)$ by treating H_t^{nn} and H_t^{nnn} on the same footing, i.e., both as the glue binding spinons to holons. This $G_\sigma^f(\omega, k)$ differs only slightly in the values of its various coefficients. Here however, we make the distinction above to keep to the original YRZ conventions of Ref. 3.

A second consequence is the absence of an anomalous spinon propagator (or at least its coherent part), consistent with an underlying assumption that spin correlations are only short-ranged in the YRZ ansatz. This form [Eq. (3)] applies in the normal phase and can be generalized to the d -wave superconducting (SC) state (e.g., see Ref. 4). Note that the YRZ theory gives a two-gap description of the pseudogap phase with separate RVB (Δ_0) and pairing Δ_{SC} gaps.

We now turn to the spin response: in the SBMFT, neglecting the effects of spinon-holon binding, this naturally takes on an RPA-like form:¹⁴

$$S(\omega, \mathbf{k}) = -\frac{3}{\pi} \text{Im} \frac{\chi_0(\omega, \mathbf{k})}{1 - J(\mathbf{k})\chi_0(\omega, \mathbf{k})}. \quad (4)$$

Here $\chi_0(\omega, \mathbf{k})$ is the bare particle-hole bubble for spinons (including anomalous contributions) and $J(\mathbf{k}) = J(\cos k_x + \cos k_y)$.

How now does our non-mean-field treatment of H_t^{nnn} alter this? First, we no longer include a contribution to χ_0 from the anomalous spinon GF. And to determine how t^{nnn} dresses the normal spinon GFs, we employ the same approximation that led to the YRZ ansatz. This means that the derivation of both $G_\sigma^f(\omega, k)$ and $S_{YRZ}(\omega, k)$ are self-consistent. Namely, we only allow diagrams involving vertices where the boson lines of the vertex are tied together. With this restriction, t^{nnn} only dresses the individual spinon propagators making up the particle-hole bubble entering χ_0 . The YRZ spin response is then

$$S_{YRZ}(\omega, \mathbf{k}) = -\frac{3}{\pi} \text{Im} \frac{\chi_{YRZ}(\omega, \mathbf{k})}{1 - J(\mathbf{k})\chi_{YRZ}(\omega, \mathbf{k})}, \quad (5)$$

where χ_{YRZ} is simply a particle-hole bubble of YRZ quasiparticles.

In computing $S_{YRZ}(\omega, \mathbf{k})$ we treat J as a fitting parameter for each doping, different from J_H . We do not expect the underlying mean-field treatment to accurately treat the renormalization of J , which is inevitably doping dependent. In particular, in the presence of strong scattering connecting the magnetic BZ boundaries, we expect J to be strongly modified. This is not merely a feature of YRZ but is generic to SB flavored theories: in Ref. 14, J had to be sharply reduced to produce an ordering transition at approximately the correct doping.

Results and discussion. We begin with the lower energy ($\omega < 100$ meV) spin response in underdoped cuprates, which has a universal hourglass shape^{1,16–18} as described in the Introduction, with a strong incommensurate response at low energies (i.e., $\omega \approx 2\Delta_{SC}$) concentrated at four points, $(\pi, \pi \pm \delta)$ and $(\pi \pm \delta, \pi)$.

We see these general features in constant-energy scans of $S_{YRZ}(\omega, \mathbf{k})$ as presented in Fig. 3 for the SC case. In this figure we have chosen parameters appropriate for the description of underdoped $\text{La}_{2-x}\text{Sr}_x\text{CuO}_4$. At very low energies ($0.05J$) the primary response is at $(\pi, \pi \pm \delta)$ and $(\pi \pm \delta, \pi)$, with $\delta = 0.16\pi$. As the energy increases there is a slight inward dispersion (δ decreases slightly), albeit in an uneven fashion

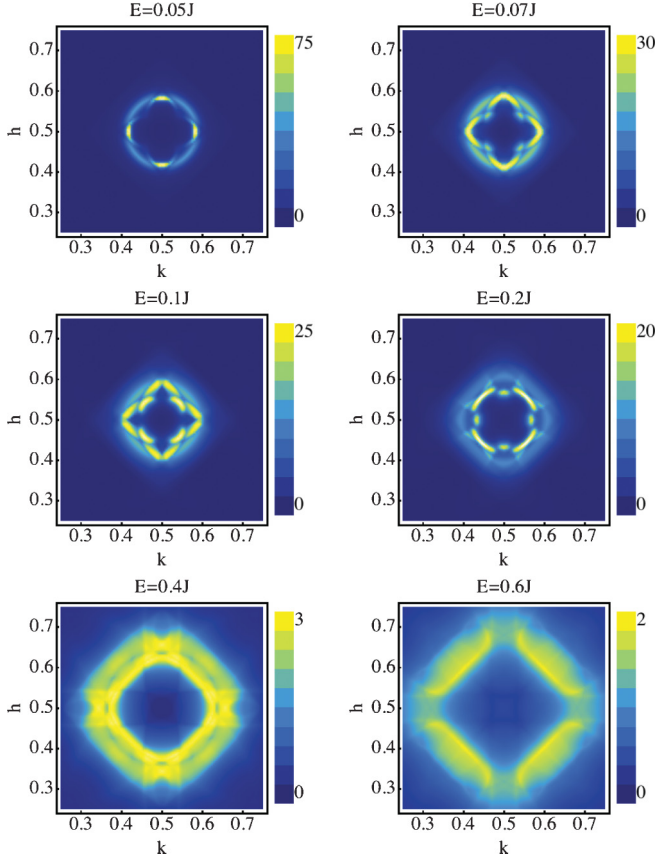


FIG. 3. (Color online) Constant energy slices of the spin response for $x = 0.12$ in the SC phase: the parameters used are the same as listed in the caption to Fig. 1, with $J = 140$ meV for our theory.

(there is a sudden movement inward at $0.125J$), with the response simultaneously becoming more isotropic (circular) about (π, π) . This dispersion reverses at $\omega \sim 0.2J$ and begins to move outwards. In this energy range the greatest response is found at about $(\pi \pm \delta', \pi \pm \delta')$. The behavior is consistent with underdoped and optimally doped $\text{La}_{2-x}\text{Sr}_x\text{CuO}_4$.^{16–18} It is also seen in stripe-stabilized $\text{La}_{2-x}\text{Ba}_x\text{CuO}_4$ ²⁰ and YBCO.^{1,19} We explicitly plot in Fig. 4(a) the \mathbf{k} point of maximal intensity as a function of the energy, comparing it with a number of cuprates.

The response found at $(\pi, \pi \pm \delta)$ and $(\pi \pm \delta, \pi)$ at $0.05J$ meV can be directly ascribed to transitions between the fronts of the pockets and the tips of the opposite pockets (vector \mathbf{Q} in Fig. 1). In general the presence of the pockets in the YRZ theory allows for low-energy scattering in a larger portion of the BZ than in theories where the spinon Fermi surface consists of four points coinciding with nodes of the SC order parameter [see Figs. 1(b) and 1(c) for a comparison of χ_{YRZ} and χ_0 ; χ_0 is the bare particle-hole bubble for the standard SB description of the spin response].¹⁴ Moreover, in the presence of an SC gap, the tips of the pockets see a saddle point in dispersion with a corresponding van Hove singularity further enhancing the low-energy scattering.

In the normal state, a low-energy spectral weight is found not just in the directions parallel to the crystal axes but also in the nodal directions (see Fig. 5). This is a result of the disappearance of the saddle point identified in Fig. 1 in the

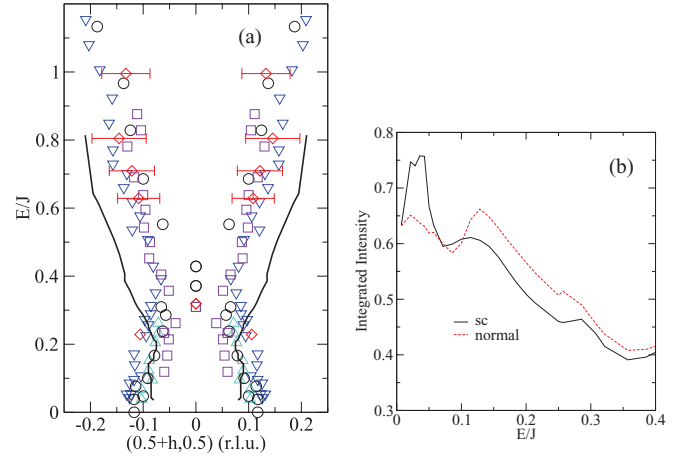


FIG. 4. (Color online) (a) Hourglass dispersion of the resonance near π, π . The thick (black) line is the position of the maximum intensity peak after integration of the numerical data over a strip of width $2\pi/25$ along the parallel direction, averaged over sections of length $2\pi/33$. Experimental data points (appropriately rescaled) are taken from^{1,19} (upward-pointing triangles) $\text{La}_{1.90}\text{Sr}_{0.10}\text{CuO}_4$,¹⁶ (circles) $\text{La}_{1.875}\text{Ba}_{0.125}\text{CuO}_4$,²⁰ (downward-pointing triangles) $\text{La}_{1.84}\text{Sr}_{0.16}\text{CuO}_4$,¹⁸ (squares) $\text{YBa}_2\text{Cu}_3\text{O}_{6.5}$,²¹ and (diamonds) $\text{YBa}_2\text{Cu}_3\text{O}_{6.6}$.²² (b) The \mathbf{k} -integrated spin response with and without a superconducting gap.

normal state. While parallel scattering still dominates at low energies, the response is less concentrated in such areas and weight does appear along the nodal directions (at least in the LSCO family).^{16,17}

Underlying our calculations of the magnetic response is the assumption that itinerant quasiparticles (even if heavily dressed) can explain this response in cuprates. While there is evidence that at least part of the spin response must be ascribed to localized spins,^{7,20} there is also evidence that impurities introduce local spins, e.g., Zn doped into YBCO²³ and earlier studies. The full cuprate magnetic response requires a mixture of the two. However, one experimental feature of the spin response that points to itinerant quasi-particles is the depression of the \mathbf{k} -integrated spin response at $\omega < 2\Delta_{\text{SC}}$ upon a decrease in $T < T_c$. This behavior is seen in both the LSCO^{16–18} and the YBCO²⁴ families and we see it in our calculations as well [Fig. 4(b)]. We also show in Fig. 4(b) that our calculated integrated intensity has a two-peak structure, with one peak at energies close to $0.05J$ and one at energies of $\approx 0.12J$. This doubling of peaks is seen in near optimally

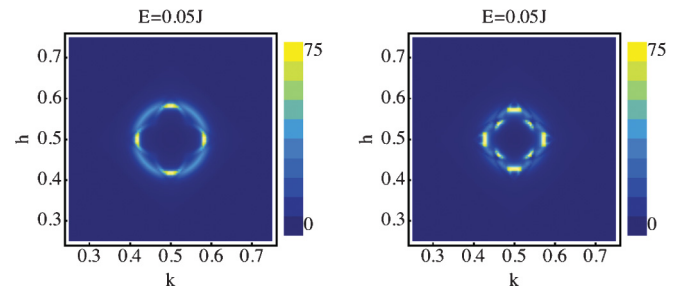


FIG. 5. (Color online) $x = 0.12$ and $\omega = 0.05J$ constant-energy slices for the SC phase (left) and the normal phase (right).

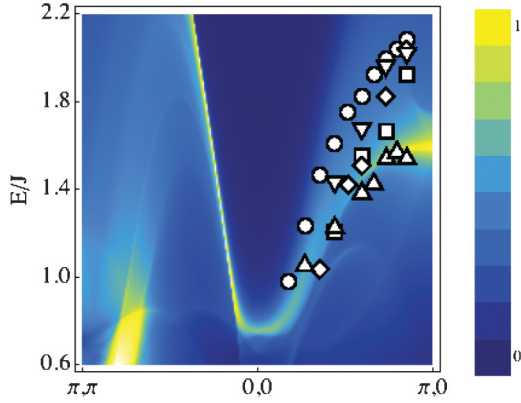


FIG. 6. (Color online) The spin response for energies from 100 to 300 meV, for cuts from (π, π) to $(0, 0)$ to $(\pi, 0)$ in the Brillouin zone (same choice of parameters as previously). Also plotted are data points from² (circles) $\text{Nd}_{1.2}\text{Ba}_{1.8}\text{Cu}_3\text{O}_6$, (squares) $\text{YBa}_2\text{Cu}_3\text{O}_7$, (diamonds) $\text{Nd}_{1.2}\text{Ba}_{1.8}\text{Cu}_3\text{O}_7$, (upward-pointing triangles) $\text{YBa}_2\text{Cu}_4\text{O}_8$, and (downward-pointing triangles) $\text{YBa}_2\text{Cu}_3\text{O}_{6.6}$. Here $J = 140$ meV.

doped LSCO.^{17,18} In underdoped LSCO at least the lower energy peak has been observed.¹⁶

Turning to high energies, $\omega > 100$ meV, we find that the YRZ spin response is able to explain key features in the spin response recently measured by RIXS. In Fig. 6 we plot the spin response for energies $100 \text{ meV} < \omega < 300 \text{ meV}$ for two cuts in the BZ. We see two features emanating

from $(0, 0)$. One disperses towards $(\pi, 0)$ as the energy is increased (corresponding well with the reported paramagnon-like excitation in the RIXS data of Ref. 2 on a variety of cuprates). The other, with a considerably higher spin velocity, evolves towards (π, π) . This dispersing paramagnon excitation naturally appears from a two-band factorization of YRZ [a simple rewriting of Eq. (3)].⁴

$$G_{\sigma}^f(\omega, \mathbf{k}) = \frac{z_{+}(\mathbf{k})}{\omega - \omega_{+}(\mathbf{k})} + \frac{z_{-}(\mathbf{k})}{\omega - \omega_{-}(\mathbf{k})}. \quad (6)$$

The paramagnon results from a particle-hole excitation from the lower band, $\omega_{-}(\mathbf{k})$, to the upper band, $\omega_{+}(\mathbf{k})$. This feature is particularly robust, as it only relies on the factorization of YRZ into two effective bands. Note that the low-energy response is primarily due to intraband transitions within the lower, $\omega_{-}(\mathbf{k})$, band.

In conclusion, we have shown that calculations of the magnetic response based on itinerant YRZ quasiparticles satisfactorily reproduce key features of experiments on the spin response of underdoped cuprates at both low and high energies.

The authors thank J. Tranquada, J. Hill, and M. Dean for useful conversations. We acknowledge support from the Center for Emergent Superconductivity, an Energy Frontier Research Center funded by the DOE Office of Science, Office of Basic Energy Science, under Award No. DE-AC0298CH1088. T.M.R. also acknowledges support from the Swiss National Science Foundation.

*Corresponding author: rmk@bnl.gov

¹For a recent review see M. Fujita *et al.*, *J. Phys. Soc. Jpn.* **81**, 011007 (2012).

²M. Le Tacon *et al.*, *Nature Phys.* **7**, 725 (2011).

³K.-Y. Yang, T. M. Rice, and F.-C. Zhang, *Phys. Rev. B* **73**, 174501 (2006).

⁴T. M. Rice, K.-Y. Yang, and F.-C. Zhang, *Rep. Prog. Phys.* **75**, 01650 (2012).

⁵A. R. Schmidt *et al.*, *New J. Phys.* **13**, 065014 (2011); Y. Kohsaka *et al.*, *Nature* **454**, 1072 (2008).

⁶H. B. Yang, J. D. Rameau, Z. H. Pan, G. D. Gu, P. D. Johnson, H. Claus, D. G. Hinks, and T. E. Kidd, *Phys. Rev. Lett.* **107**, 047003 (2011).

⁷G. Xu *et al.*, *Nature Phys.* **5**, 642 (2009).

⁸M. Vojta, *Nature Phys.* **5**, 623 (2009); **7**, 674 (2011).

⁹G. S. Uhrig *et al.*, *J. Phys. Soc. Jpn.* **74**, Suppl. 86 (2005).

¹⁰M. Vojta, *Adv. Phys.* **58**, 699 (2009).

¹¹Private communication from P. A. Lee. P. A. Lee's suggestion is in turn based on T. K. Ng, *Phys. Rev. B* **71**, 172509 (2005).

¹²C. Honerkamp, M. Salmhofer, N. Furukawa, and T. M. Rice, *Phys. Rev. B* **63**, 035109 (2001).

¹³R. M. Konik, T. M. Rice, and A. M. Tsvelik, *Phys. Rev. Lett.* **96**, 086407 (2006).

¹⁴J. Brinckmann and P. A. Lee, *Phys. Rev. B* **65**, 014502 (2001).

¹⁵See Supplemental Material at <http://link.aps.org/supplemental/10.1103/PhysRevB.86.100508> for a derivation of YRZ that treats NN and further hopping terms on an equal footing.

¹⁶O. J. Lipscombe, B. Vignolle, T. G. Perring, C. D. Frost, and S. M. Hayden, *Phys. Rev. Lett.* **102**, 167002 (2009).

¹⁷N. B. Christensen, D. F. McMorrow, H. M. Ronnow, B. Lake, S. M. Hayden, G. Aeppli, T. G. Perring, M. Mangorntong, M. Nohara, and H. Tagaki, *Phys. Rev. Lett.* **93**, 147002 (2004).

¹⁸B. Vignolle *et al.*, *Nature Phys.* **3**, 163 (2007).

¹⁹J. Tranquada, in *Handbook of High-Temperature Superconductivity: Theory and Experiment*, edited by J. R. Schrieffer (Springer, New York, 2007).

²⁰J. M. Tranquada *et al.*, *Nature* **429**, 534 (2004).

²¹C. Stock *et al.*, *Phys. Rev. B* **71**, 024522 (2005).

²²S. M. Hayden *et al.*, *Nature* **429**, 531 (2004).

²³A. Suchanek *et al.*, *Phys. Rev. Lett.* **105**, 037207 (2010).

²⁴C. Stock, W. J. L. Buyers, R. Liang, D. Peets, Z. Tun, D. Bonn, W. N. Hardy, and R. J. Birgeneau, *Phys. Rev. B* **69**, 014502 (2004).